Materials Science in Semiconductor Processing 26 (2014) 251–258

Contents lists available at ScienceDirect

Materials Science in Semiconductor Processing

journal homepage: www.elsevier.com/locate/mssp

Sol–gel derived nanocrystalline TiO_2 thin films: A promising candidate for self-cleaning smart window applications

S.R. Meher*, L. Balakrishnan

School of Advanced Sciences, VIT University, Vellore 632014, India

ARTICLE INFO

Keywords:
TiO_2 thin films
Sol–gel
Semiconductors
Photocatalysis
Electrochromism

ABSTRACT

In the present work, anatase TiO_2 films are prepared by sol–gel spin coating method. The structural and optical properties of the films have been studied at different post-annealing temperatures. The photocatalytic activity and electrochromic performance of the films are investigated. The films annealed at 400 °C exhibit the highest photocatalytic activity with a rate constant of 4.56×10^{-3} min^{-1}. The electrochromic performance for the films annealed at 400 °C expressed in terms of difference in optical density (ΔOD) at 550 nm between coloured and bleached state is 0.5493. This combination of photocatalysis and electrochromism makes the sol–gel derived titania thin films as promising candidates for self-cleaning smart window applications.

1. Introduction

Anatase titania (TiO_2) has been studied extensively in last few decades for its high efficiency photocatalytic properties [1–3]. Moreover, its biocompatibility and low cost factor are added advantages for real time applications. Therefore, among many candidates for photocatalysis, TiO_2 is considered as the only material which is industrially reliable. The photocatalytic properties of TiO_2 were first realized in 1980s for the detoxication of various harmful compounds both in water and air. In the photocatalytic process, electron–hole pairs are generated when TiO_2 is photo-activated with ultraviolet (UV) light having an energy higher than its band gap [1]. The electrons and holes are used in the red-ox breakdown of organic pollutants leaving CO_2 and other mineral acids as the residue. The holes generated in TiO_2 are highly oxidising and most organic compounds are completely oxidised by it. In the literature, the enhanced photocatalytic activity exhibited by nanocrystalline TiO_2 films is mainly attributed to the increase in surface to volume ratio which results in more number of active sites and the quantum confinement effect [4]. Though, TiO_2 is widely studied and mostly used as a photocatalytic material, its electrochromic properties have not been explored extensively [5–7] as compared to other transient metal oxides like WO_3 [8], Nb_2O_5 [9] and V_2O_5 [10]. The most accepted model [11] for electrochromic reaction in TiO_2 is the injection of electrons, followed by intercalation of monovalent ions into an oxide matrix.

$$\underset{\text{(Colourless)}}{TiO_2} + xe^- + xM^+ \rightleftarrows \underset{\text{(Coloured)}}{M_xTiO_2} \quad (1)$$

where, M^+ is a monovalent ion (H^+, Li^+, Na^+) and x can vary between 0 and 1.

There is no correlation between the electrochromic and photocatalytic phenomena and both are considered to be entirely independent of each other. The electrochromic behaviour is due to the charge intercalation into the lattice resulting in colour change whereas photocatalysis is related to the creation of electron–hole pairs on the semiconductor surface. But, a good combination of photocatalytic and electrochromic properties is desirable for self-cleaning smart window applications. The combination of photocatalysis and electrochromism in a single material allows us for

* Corresponding author. Tel.: +91 416 2202717.
E-mail address: samirmeher@gmail.com (S.R. Meher).

http://dx.doi.org/10.1016/j.mssp.2014.05.006
1369-8001/

a one-step, cost-effective and high throughput growth process in the fabrication of self-cleaning smart windows. In these applications, the self-cleaning mechanism works in two stages. The primary and important stage is breaking down of the organic contaminants through photocatalytic activity. This makes the glass surface superhydrophilic which reduces the water contact angle. In the superhydrophilic stage, water forms a thin layer on glass and the dirt is washed away. On the other hand, smart windows work on the principle of electrochromism. Smart windows not only block the visible light but also absorb the near-infrared (NIR) light which is invisible but produces heat.

Hence, the main objective of the present work is to look for a good combination of photocatalytic and electrochromic behaviours of nano-crystalline anatase TiO_2 thin films. In the literature, several deposition methods like radio-frequency magnetron sputtering [12], reactive magnetron sputtering [13], pulsed laser deposition [14], reactive e-beam evaporation [15], spray pyrolysis [16], sol–gel spin coating [17,18] etc. has been prescribed for the growth of TiO_2 thin films. Out of these techniques, sol–gel has got distinct advantage from others due to the atomic scale mixing of the constituents, ease of operation and cost factor [19]. Therefore, in the present work, we have prepared nano-crystalline TiO_2 thin films by the sol–gel spin coating method and have studied their photocatalytic properties at different post-annealing temperatures. The films showing the best photocatalytic property have been checked for their electrochromic behaviour.

2. Experimental details

TiO_2 thin films were prepared by the sol–gel spin coating method. Titanium iso-propoxide ($Ti(OC_3H_7)_4$) was used as the titanium precursor and ethanol as the solvent. The flow chart for the preparation steps is shown in Fig. 1. Titanium ion concentration was kept at 0.2 M. The films were deposited by spin coating on borosilicate glass (BSG), ITO (10% Sn doped In_2O_3) coated glass and *p*- type Si (100) substrates. Six layers of TiO_2 thin films were deposited in order to obtain the desired uniform thickness for all the samples. After coating each layer, the films were pre-heated at 250 °C for 5 min in air. Finally, all the films were annealed at different temperatures for 1 h in air.

Grazing angle X-ray diffraction (GAXRD) measurements were carried out using a Phillips X'Pert Pro diffractometer with Cu Kα radiation ($\lambda = 1.5418$ Å) at a grazing angle of 2°. Raman spectra were obtained through a HORIBA Jobin Yvon Raman instrument using He–Ne laser light source (632.8 nm). Scanning electron micrographs were recorded using a field-emission scanning electron microscope (FE-SEM), FEI Quanta 200. The transmittance spectra in the wavelength range 300–2500 nm were recorded using a JASCO double beam UV–vis-NIR spectrophotometer (Model: V-570).

The photocatalytic behaviour of the films was studied by degrading Rhodamine-B (RhB) dye which is a typical pollutant in the effluent stream of dye industry. 5 cm^2 TiO_2 film was immersed in 10 ml aqueous RhB solution (0.5 mg/l). 6 W mercury tube lamp (central wavelength ~352 nm) kept at a distance of 8 cm from the film was used as the UV source. The photocatalytic activity was evaluated by measuring the changes in the optical absorbance of RhB solution in the wavelength range 400–800 nm. The electrochromic property for TiO_2 films deposited on ITO coated glass substrates was evaluated using cyclic voltametry (CV) (CH Instruments model: CHI7081C) in the three electrode electrochemical workstation by

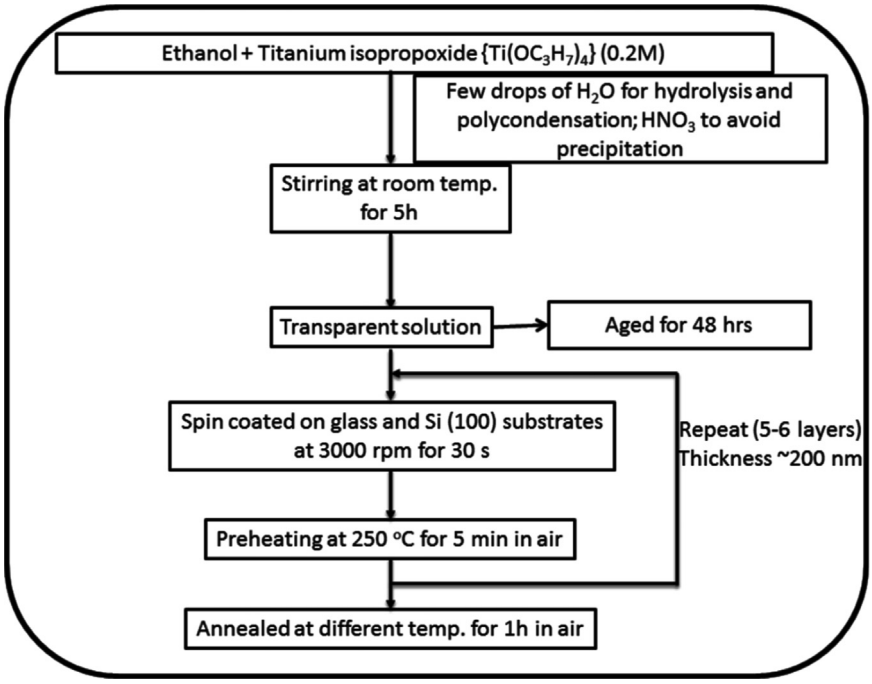

Fig. 1. Flow chart for the preparation of TiO_2 thin films by sol–gel spin coating.

sweeping the potential between −1.5 V to +1 V; the reference and auxiliary electrodes being the standard calomel electrode (SCE) and platinum wire, respectively. The measurements were performed in a liquid electrolyte (1.0 M $LiClO_4$ in propylene carbonate solution). The area of the working electrode was $1 \times 1\ cm^2$. The scan rate was kept at 50 mV/s. Again, the transmittance spectra in the coloured (−1.5 V/SCE) and bleached (+1.0 V/SCE) states were recorded using the spectrophotometer in the wavelength range 300–1000 nm.

3. Results and discussion

Fig. 2a shows the GAXRD pattern of TiO_2 films deposited on Si substrates and post-annealed at different temperatures. All the films are found to be polycrystalline in nature. No peaks corresponding to crystalline Si are observed due to the glancing angle geometry. The anatase nature of TiO_2 starts to appear at 350 °C and is maintained upto temperatures greater than 750 °C. All the films are found to have preferential growth along (101) direction. A small intensity peak at 27.6° corresponding to rutile phase is observed for the films annealed at 900 °C. The

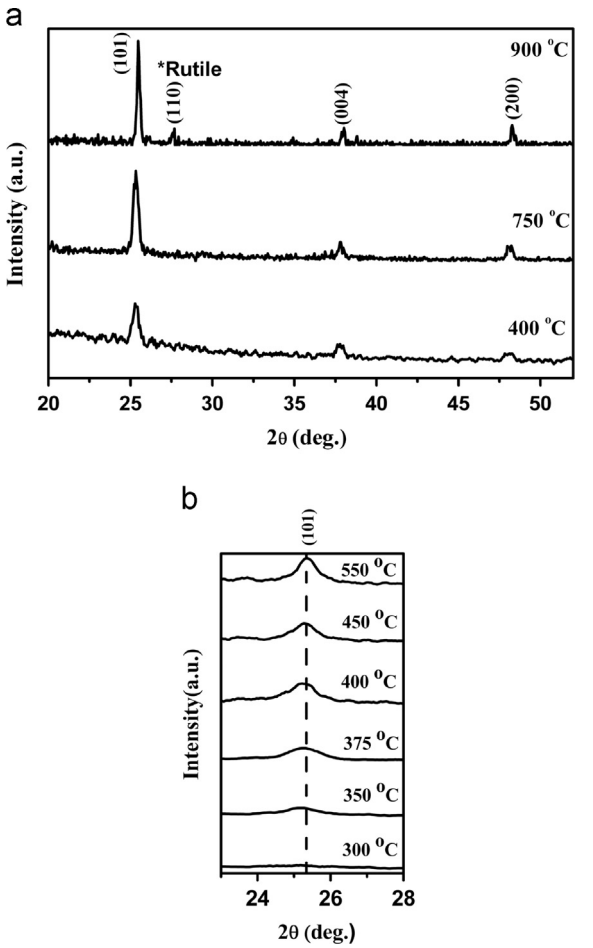

Fig. 2. (a) GAXRD pattern for TiO_2 films grown on Si substrates (b) Slow scans for the GAXRD patterns of TiO_2 films around (101) reflection grown on glass substrates at different annealing temperatures.

slow scan XRD patterns (around (101) Bragg reflection) for the films deposited on glass substrates and annealed at different temperatures are shown in Fig. 2b. We can observe that anatase phase starts appearing at 350 °C and is maintained upto higher temperatures. The crystallinity of the films improves with increase in the annealing temperature which is clearly seen from the intensity of (101) diffraction peak. The average crystallite size was calculated using Scherrer's semi-empirical formula,

$$D = \frac{0.9\lambda}{\beta \cos \theta} \tag{2}$$

where, $\lambda = 1.5418$ Å and $\beta = B - b$ (B being the observed FWHM and b is the instrument function determined from the broadening of the monocrystalline silicon diffraction line). All the films are found to be nanocrystalline in nature. The average crystallite size increases from 12 to 20 nm with increase in the annealing temperature from 350 to 550 °C. The films deposited on ITO coated glass substrates also crystallise in anatase phase. No ITO peaks could be detected in the GAXRD pattern (not shown here) due to high thickness of TiO_2 deposited on it.

The Raman spectra at room temperature in the spectrum range 100–700 cm^{-1} for TiO_2 films coated on glass substrates and annealed at different temperatures are shown in Fig. 3a. The Raman spectra were recorded in the backscattering geometry. Four well defined peaks at 143, 396, 516 and 637 cm^{-1} are observed for all the films. These peaks correspond to E_g (ν_6), B_{1g} (ν_4), $A_{1g}+B_{1g}$ ($\nu_2+\nu_3$) and E_g (ν_1) optical vibration modes. All these peaks are characteristics of the anatase phase of TiO_2 [20,21]. The differences with literature values are reasonable due to the possibility of structural distortions or inter-grain defects present in the sample. 143 cm^{-1} Raman peak is the most intense and it corresponds to E_g mode of anatase TiO_2. The area and FWHM of 143 cm^{-1} peak is plotted as a function of annealing temperature in Fig. 3b. The increase in area and decrease in FWHM of this peak with annealing temperature further confirms the fact that annealing leads to an improvement in the crystalline quality of the films.

Fig. 4 shows the UV–vis-NIR transmission spectra of TiO_2 films coated on glass substrates and annealed at different temperatures. All the films are highly transparent (~80%) in the visible and NIR region with a sharp absorption edge in the UV region. The high transmittance indicates fairly smooth surface and relatively good film homogeneity. The sharp absorption edge is shown in the inset with the black solid line representing the transmittance for glass substrate.

Refractive indices in the wavelength range 400–700 nm for TiO_2 films under investigation were calculated by the envelope method [22]. The envelopes can be drawn through the maxima (T_M) and minima (T_m) of the transmittance curve using the following relation.

$$n_f = \sqrt{N + \sqrt{N^2 - n_s^2}} \tag{3}$$

where,

$$N = 2n_s \frac{T_M - T_m}{T_M T_m} + \frac{n_s^2 + 1}{2} \tag{4}$$

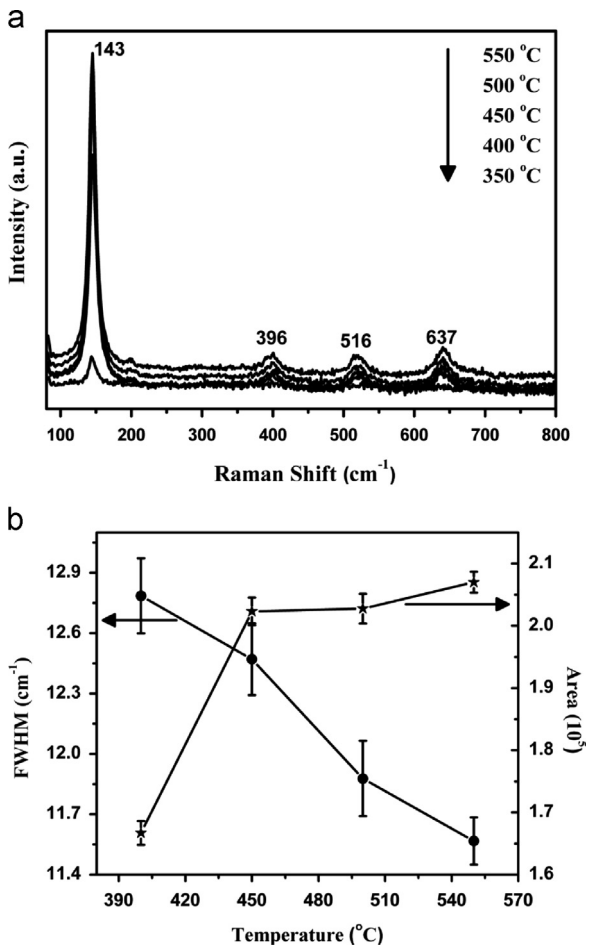

Fig. 3. (a) Raman spectra for TiO_2 films grown on glass substrates and annealed at different temperatures. (b) Plot of area and FWHM for 143 cm^{-1} Raman peak as a function of annealing temperature (Solid line drawn is a guide to the eye).

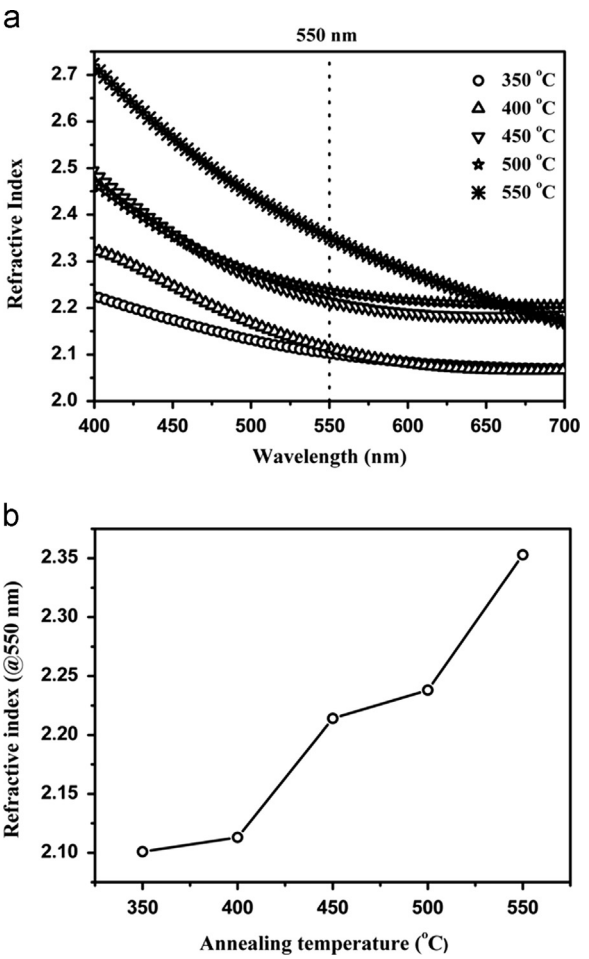

Fig. 5. (a) Refractive index of titania films as a function of wavelength (b) Variation of refractive index of titania films at 550 nm as a function of annealing temperature (Solid line drawn is a guide to the eye).

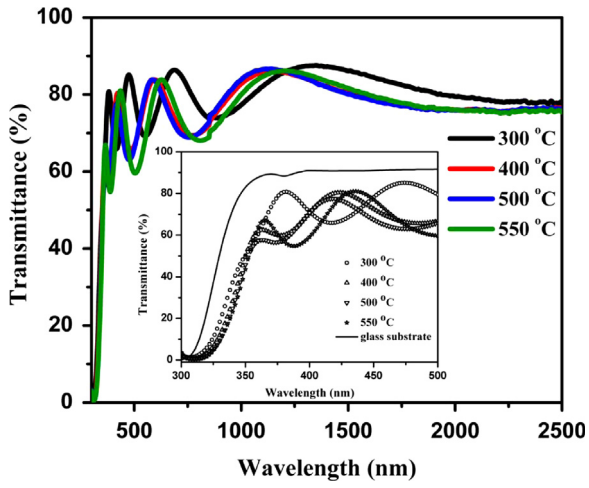

Fig. 4. UV–vis-NIR transmission spectra for anatase titania films deposited on glass substrates and annealed at different temperatures. Inset shows the sharp absorption edge.

Here, n_s stands for refractive index of the substrate (glass = 1.5). The refractive index decreases with increase in the wavelength for all the films (Fig. 5a). The refractive index at 550 nm increases with increase in the annealing temperature (Fig. 5b). It is mainly due to the increase in the grain size and proper densification of grains. The thicknesses (d) of the films were calculated using the following relation:

$$d = \frac{\lambda_1 \lambda_2}{2(\lambda_1 n_2 - \lambda_2 n_1)} \tag{5}$$

where, n_1 and n_2 are the refractive indices at two adjacent maxima (or minima) at λ_1 and λ_2. The thickness for all the films lies between 200 and 300 nm.

For highly transparent films, the absorption coefficient (α) and the transmittance (T) can be related as,

$$\alpha = \frac{-\ln T}{d} \tag{6}$$

where, d is the film thickness. The relation between the absorption coefficient and incident energy can be expressed

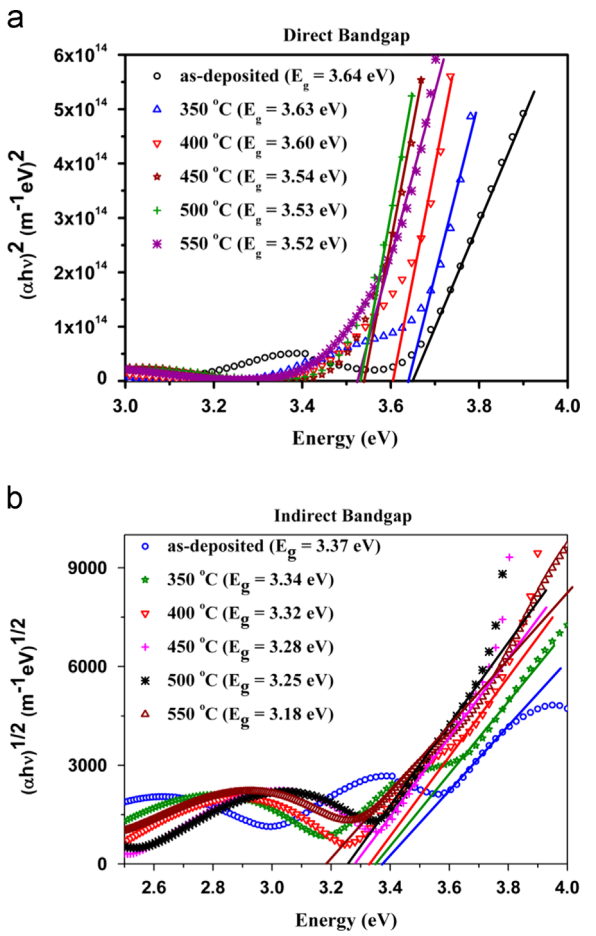

Fig. 6. Plot of (a) $(\alpha h\nu)^2$ versus $h\nu$ and (b) $(\alpha h\nu)^{1/2}$ versus $h\nu$ for direct and indirect band gap determination, respectively at different annealing temperatures.

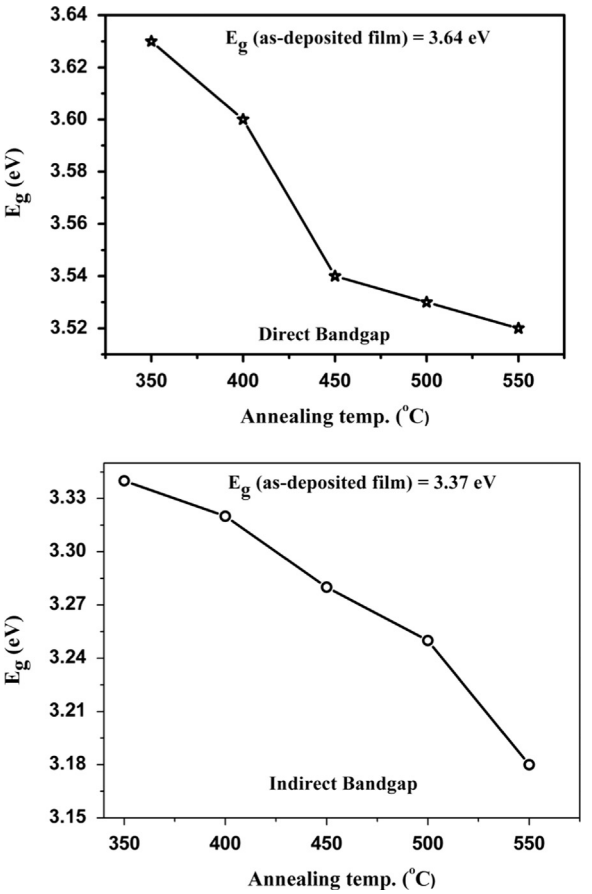

Fig. 7. Annealing temperature dependence of the direct and indirect band gaps of TiO_2 films (Solid lines drawn are guide the eye).

as Eqs. (7) and (8) for direct and indirect transitions, respectively, where A_1 and A_2 are constants and E_{g1} and E_{g2} are direct and indirect band gaps, respectively [23].

$$\alpha h\nu = A_1(h\nu - E_{g1})^{1/2} \tag{7}$$

$$\alpha h\nu = A_2(h\nu - E_{g2})^{2} \tag{8}$$

The reports on band to band transition in anatase TiO_2 are highly debatable. In a direct band gap semiconductor, the conduction band minimum and valence band maximum have the same crystal momentum. This results in a fast recombination of the electron–hole pair. In an indirect band gap semiconductor, the conduction band edge and valence band edge have different crystal momenta which enables the excited electron to stabilise at the lower level in the conduction band leading to longer life and higher mobility. Hence, indirect transition is more advantageous for photocatalytic activity. There are very few ab-initio band structure calculations available in the literature for anatase TiO_2 and most of them assign an indirect band to band transition [24,25]. But, the band structures obtained from ab-initio calculations are for infinitely ordered single crystals at absolute zero temperature which may not be exactly the same for polycrystalline thin films at room temperature. The band structure for polycrystalline thin films is expected to be distorted because of the presence of grain boundaries. The room temperature will also introduce some band tailing effects. This is the reason for ambiguous reports on the nature of band to band transition in anatase TiO_2 thin films i.e. many studies assume an indirect band gap [26,27] where as many others assume a direct band gap [12,28,29]. Moreover, recently Luttrell et al. [30] have also obtained indirect as well as direct band gaps for epitaxial anatase TiO_2 films.

Therefore, in the present study due to absence of any concrete knowledge about the band structure of sol–gel derived nanocrystalline anatase TiO_2 films, we have evaluated the band gaps assuming both direct and indirect transitions. The $(\alpha h\nu)^2$ (for direct) and $(\alpha h\nu)^{1/2}$ (for indirect) versus $h\nu$ plots are shown in Figs. 6a and b, respectively. The direct and indirect band gap values were determined by extrapolating the linear part of the curve to $\alpha = 0$. A direct band gap of 3.64 eV and an indirect band gap of 3.37 eV were obtained for as-deposited films. Both direct and indirect band gap values decrease with increase in annealing temperature (Fig. 7) which is mainly attributed to increase in grain size and relaxation of built-in tensile strain in the films with annealing temperature.

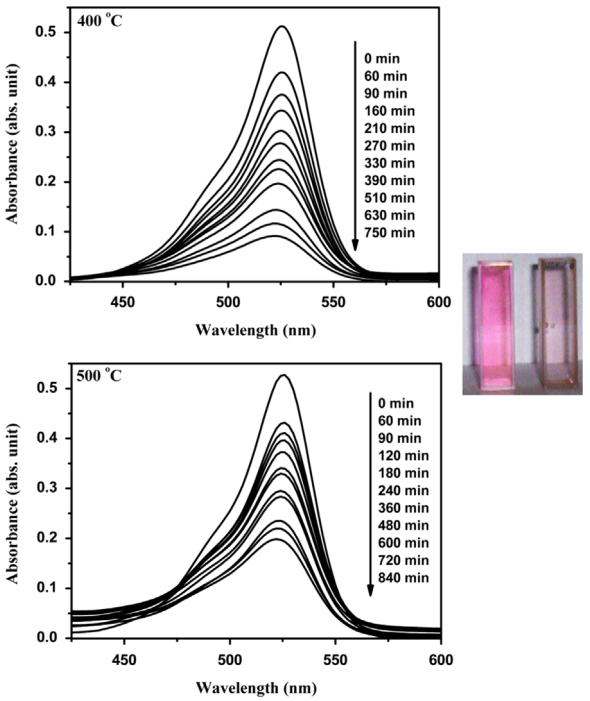

Fig. 8. Optical absorbance of RhB solution at different UV irradiation time in the presence of TiO_2 photocatalyst annealed at 400 °C and 500 °C; Change in the colour of RhB solution from pink to nearly colourless. (For interpretation of the references to color in this figure legend, the reader is referred to the web version of this article.)

3.1. Photocatalytic performance

The photocatalytic activity of titania films annealed at different temperatures was evaluated by studying the decomposition of RhB dye solution. The change in RhB concentration in accordance with irradiation time was measured by measuring its absorption spectrum using a spectrophotometer. RhB dye exhibits a strong absorption around 500–550 nm which results in a broad asymmetric peak. The absorbance was found to be decreasing with increase in UV irradiation time in the presence of titania photocatalyst (Fig. 8a). The colour of RhB solution changes from pink to nearly colourless (Fig. 8b) which indicates photocatalytic reaction. Fig. 9a shows the percentage change in RhB concentration as a function of irradiation time. The films annealed at 400 °C show the maximum degradation efficiency of 98% after an irradiation time of 12.5 h.

The increase in photocatalytic efficiency can be partly attributed to the increase in the specific surface area of these nanocrystalline films which results in more number of reactive sites to absorb pollutants. In addition to this, the diffusion of photo-induced carriers from bulk to surface becomes fast with decrease in crystallite size [31] leading to increased photocatalysis. Again, annealing releases the internal stress and improves crystallinity, which also helps in enhancing the photocatalytic activity. At the same time, crystallite size increases with increase in annealing temperature which has a negative impact on the photocatalytic activity. Hence, enhancement in the photocatalytic activity in the present study can be explained as a competing mechanism between the small size effect and improved crystallinity. The plot of $\ln(C_0/C)$ versus irradiation time (Fig. 9b) is linear. Hence, it can be concluded that photocatalytic degradation follows the pseudo first order reaction kinetics [32]. The half-life period of disintegration and the rate constant were

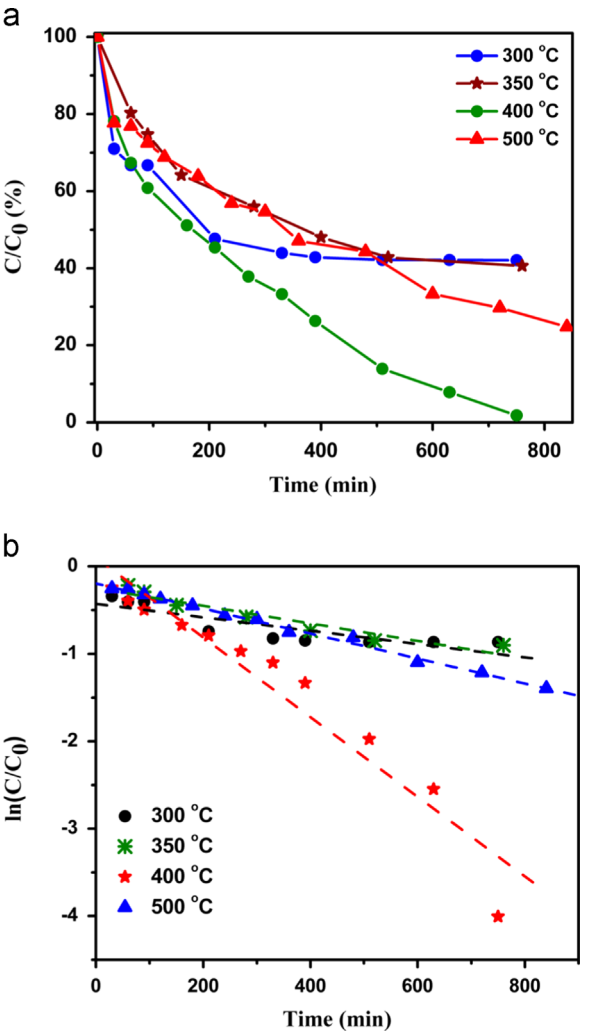

Fig. 9. (a) Percentage change in RhB concentration as a function of irradiation time for TiO_2 photocatalysts annealed at different temperatures. (b) Plot of $\ln(C_0/C)$ versus irradiation time for TiO_2 films annealed at different temperatures.

Table 1
Photocatalytic activity and crystallite size at different annealing temperatures.

Annealing Temp. (°C)	Rate constant (10^{-3} min^{-1})	Half-life ($_{min}$)	Crystallite size (nm)
300	1.73	400.5	Amorphous
350	0.988	700.9	12.4
400	4.56	151.9	15.7
500	1.43	484.6	19.8

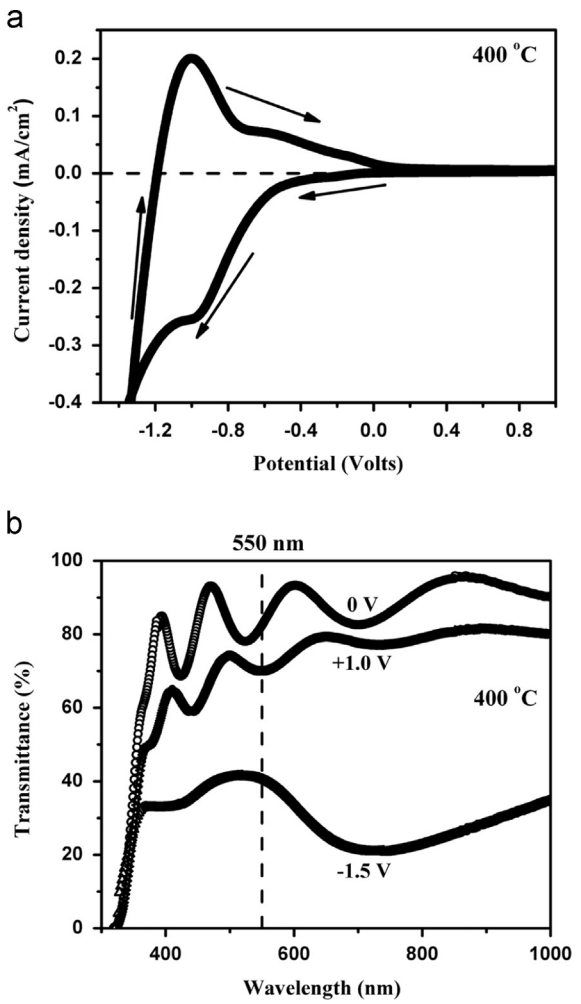

Fig. 10. (a) CV curve for TiO_2 films deposited on ITO coated glass substrates (in $LiClO_4$+PC solution) and annealed at 400 °C. (b) Transmittance spectra in the open circuit, coloured state and bleached state.

calculated from reaction kinetics and are given in Table 1. Since, TiO_2 films annealed at 400 °C exhibit the highest rate constant of 4.56×10^{-3} min^{-1} ($t_{1/2}$=151.9 min), they were further studied for their electrochromic properties.

3.2. Electrochromic performance

Fig. 10a shows the cyclic voltammetry curve for titania films (deposited on ITO coated glass substrates and annealed at 400 °C) in $LiClO_4$+Propylene carbonate solution. A cathodic electronic current (electrons flow into TiO_2 film) arises under the application of cathodic potential from the cell equilibrium potential. The colour of the film turns greyish and is opaque to ordinary human eye. An anodic electronic current (electrons flow out of TiO_2 film [33]) is established by reversing the direction of anodic potential. The film bleaches to its initial colour state in a cyclic process. The reduction peak is observed at −1.0 V (0.20 mA/cm^2) whereas two oxidation peaks are observed at −0.97 V (−0.24 mA/cm^2) and −1.32 V (−0.36 mA/cm^2), respectively. The saturated state of the colour was achieved in less than 10 s after a negative potential of −1.5 V /SCE was applied to working electrode. The transmittance spectra obtained during colouration at a polarised potential of −1.5 V/SCE are given in Fig. 10b. The transmittance spectra for open circuit (0 V) and for bleached state (+1.0 V/SCE) are also shown in the same figure. The electrochromic performance of titania films annealed at 400 °C was evaluated by using the differences in optical density (ΔOD) derived from the two transmittance spectra taken at 550 nm for coloured (−1.5 V/SCE) and bleached (+1.0 V/SCE) states. ΔOD was calculated by using the equation [6]:

$$\Delta OD = \ln\left(\frac{T_{bleached}}{T_{Coloured}}\right) \quad (9)$$

The value of ΔOD (at 550 nm) for the sample under investigation was found to be 0.5493. The corresponding transmittance variation (at 550 nm) between the coloured and bleached state is ~30% which is suitable enough for smart window applications.

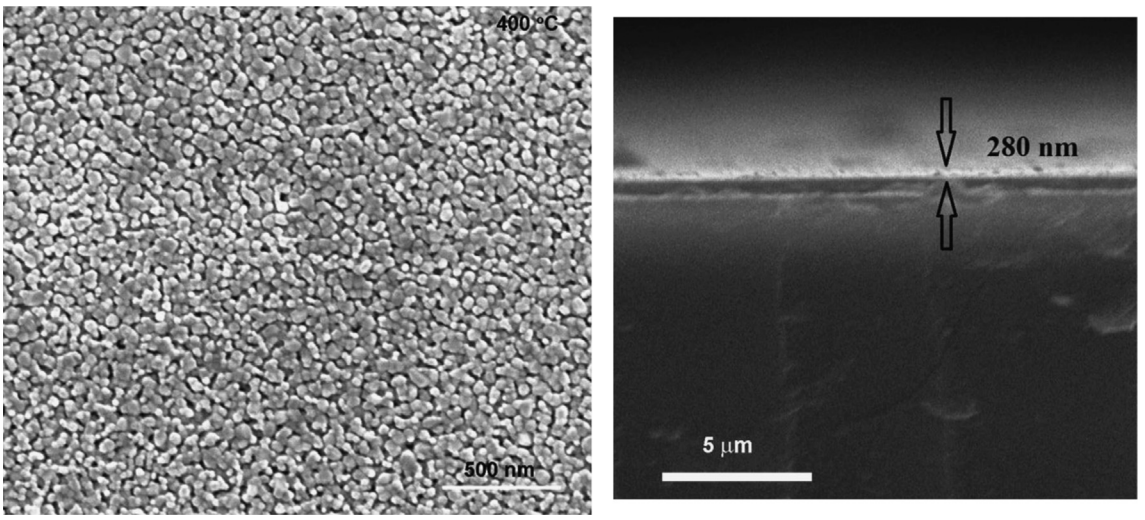

Fig. 11. FE-SEM figures (top-view and cross-sectional view) of TiO_2 films annealed at 400 °C.

3.3. Surface morphology

The FE-SEM micrograph of TiO_2 films annealed at 400 °C is shown in Fig. 11. The top-view micrograph shows well-defined randomly oriented grains. The average grain size was found to be 36 nm. The grains are closely packed without any visible pores between them. The grain size obtained from SEM is not in agreement with the average crystallite size (~16 nm) obtained from XRD. It is because the crystallites contain some amount of amorphous phase surrounding them which cannot be detected by XRD. From the cross-sectional view, the thickness of the films was found to be ~280 nm with good uniformity.

4. Conclusion

Commercially viable and cost-effective, sol–gel spin coating method was used to deposit titania thin films on glass, Si and ITO coated glass substrates. The films are found to crystallise in anatase form up to temperatures higher than 750 °C. Raman spectroscopy measurements also confirm the anatase phase of TiO_2. The direct and indirect band gaps of the films obtained from transmittance spectra are found to decrease with increase in annealing temperature which is mainly attributed to the relaxation of built in tensile strain. The increase in the refractive index with annealing temperature refers to proper densification of grains. Further the films were studied for their photocatalytic and electrochromic performances. The films annealed at 400 °C are found to have the maximum photocatalytic efficiency with a rate constant of 4.56×10^{-3} min^{-1}. The electrochromic performance of the films deposited on ITO coated glass substrates and annealed at 400 °C was investigated using CV measurements. The difference in optical density (ΔOD) between the coloured and bleached state is found to be 0.5493. From SEM micrograph, the continuity and thickness uniformity of the films is observed. In conclusion, sol–gel derived anatse TiO_2 films annealed at 400 °C show the best UV photocatalytic activity and a reasonably good electrochromic performance. Hence, these films are promising candidates to be used in self-cleaning smart window applications. Nevertheless, their hydrophilic behaviour needs to be checked for complete self-cleaning action.

Acknowledgement

The authors would like to acknowledge Department of Physics, I.I.T. Madras, India, for providing necessary infrastructure to carry out this work.

References

[1] K. Hashimoto, H. Irie, A. Fujishima, Jpn. J. Appl. Phys. 44 (2005) 8269–8285.
[2] K. Nakata, A. Fujishima, J. Photochem. Photobiol. C 13 (2012) 169–189.
[3] A. Fujishima, X. Zhang, D.A. Tryk, Surf. Sci. Rep. 63 (2008) 515–582.
[4] H. Lin, C.P. Huang, W. Li, C. Ni, S.I. Shah, Y.H. Tseng, Appl. Catal. B 68 (2006) 1–11.
[5] N.N. Dinh, N.M. Quyen, D.N. Chuang, M. Zikova, V.V. Truong, Sol. Energy Mater. Sol. Cells 95 (2011) 618–623.
[6] S.Y. Lin, Y.C. Chen, C.M. Wang, C.C. Liu, J. Solid State Electrochem. 12 (2008) 1481–1486.
[7] I. Sorar, E. Pehlivan, G.A. Niklasson, C.G. Granqvist, Sol. Energy Mater. Sol. Cells 115 (2013) 172–180.
[8] C.G. Granqvist, Sol. Energy Mater. Sol. Cells 60 (2000) 201–262.
[9] R. Romero, E.A. Dalchiele, F. Martin, D. Leinen, J.R. Ramos-Barrado, Sol. Energy Mater. Sol. Cells 93 (2009) 222–229.
[10] L. Ottaviano, A. Pennisi, F. Simone, A.M. Salvi, Opt. Mater. 27 (2004) 307–313.
[11] G. Campet, J. Portier, S.J. Wen, B. Morel, M. Bourrel, J.M. Chabagno, Act. Passiv. Electron. Compon. 14 (1992) 225–231.
[12] M. Selmi, F. Chaabouni, M. Abaab, B. Rezig, Phys. Status Sol. C 5 (2008) 3368–3372.
[13] S. Boukrouh, R. Bensaha, S. Bourgeois, E. Finot, M.C. Marco de Lucas, Thin Solid Films 516 (2008) 6353–6358.
[14] F. Gamez, A. Plaza-Reyes, P. Hurtado, E. Guillen, J.A. Anta, B. Martinez-Haya, J. Phys. Chem. C 114 (2010) 17409–17415.
[15] O. Duyar, F. Placido, H.Z. Durusoy, J. Phys. D: Appl. Phys. 41 (2008). (095307-1–7).
[16] M.D. Blesic, Z.V. Saponjic, J.M. Nedeljkovic, D.P. Uskokovic, Mater. Lett. 54 (2002) 298–302.
[17] K.P. Biju, M.K. Jain, Thin Solid Films 516 (2008) 2175–2180.
[18] A. Ranjitha, N. Muthukumarasamy, M. Thambidurai, R. Balasundaraprabhu, S. Agilan, Optik 124 (2013) 6201–6204.
[19] S.R. Meher, K.P. Biju, M.K. Jain, J. Sol-Gel Sci. Technol. 52 (2009) 228–234.
[20] T. Oshaka, F. Izumi, Y. Fujiki, J. Raman Spectrosc. 7 (1978) 321–324.
[21] B. Liu, L. Wen, X. Zhao, Mater. Chem. Phys. 106 (2007) 350–353.
[22] R. Swanepoel, J. Phys. E: Sci. Instrum. 16 (1983) 1214–1222.
[23] J. Tauc, R. Grigorovici, A. Vancu, Phys. Status Solidi B 15 (1966) 627–637.
[24] M. Landmann, E. Rauls, W.G. Schmidt, J. Phys.: Condens. Matter 24 (2012). (195503-1–6).
[25] R. Sanjines, H. Tang, H Berger, F. Gozzo, G. Margaritondo, F. Levy, J. Appl. Phys. 75 (1994) 2945–2951.
[26] D.Y. Lee, J.T. Kim, J.H. Park, Y.H. Kim, I.K. Lee, M.H. Lee, B.Y. Kim, Curr. Appl. Phys. 13 (2013) 1301–1305.
[27] C.P. Lin, H. Chen, A. Nakaruk, P. Koshy, C.C. Sorrell, Energy Procedia 34 (2013) 627–636.
[28] M.N. Ghazzal, N. Chaoui, M. Genet, E.M. Gaigneaux, D. Robert, Thin Solid Films 520 (2011) 1147–1154.
[29] K.M. Reddy, S.V. Manorama, A.R. Reddy, Mater. Chem. Phys. 78 (2002) 239–245.
[30] T. Luttrell, S. Halpegamage, J. Tao, A. Kramer, E. Sutter, M. Batzill, Sci. Rep. 4 (2014). (4043-1–8).
[31] J. Nelson, Phys. Rev. B 59 (1999) 15374–15380.
[32] D. Chen, A.K. Ray, Appl. Catal. B 23 (1999) 143–157.
[33] J. Scarminio, A. Urbano, B. Gardes, Mater. Chem. Phys. 61 (1999) 143–146.